

Experimental determination of *Philodendron melinonii* and *Arabidopsis thaliana* tissue microstructure and geometric modeling via finite-edge centroidal Voronoi tessellation

Tanvir R. Faisal,^{1,*} Nicolay Hristozov,^{2,†} Alejandro D. Rey,^{3,‡} Tamara L. Western,^{2,§} and Damiano Pasini^{1,||}

¹*Department of Mechanical Engineering, McGill University, 817 Sherbrooke St. West, Montreal, QC H3A 0C3, Canada*

²*Department of Biology, McGill University, QC H3A 1B1, Canada*

³*Department of Chemical Engineering, McGill University, QC H3A 2B2, Canada*

(Received 21 May 2012; revised manuscript received 9 August 2012; published 26 September 2012)

Plant petioles and stems are hierarchical cellular structures, displaying structural features defined at multiple length scales. One or more of the intermediate hierarchical levels consists of tissues, in which the cellular distribution is quasirandom. The current work focuses on the realistic modeling of plant tissue microstructures. The finite-edge centroidal Voronoi tessellation (FECVT) is here introduced to overcome the drawbacks of the semi-infinite edges of a typical Voronoi model. FECVT can generate a realistic model of a tissue microstructure, which might have finite edges at its border, be defined by a boundary contour of any shape, and include complex heterogeneity and cellular gradients. The centroid-based Voronoi tessellation is applied to model the microstructure of the *Philodendron melinonii* petiole and the *Arabidopsis thaliana* stem, which both display intense cellular gradients. FECVT coupled with a digital image processing algorithm is implemented to capture the nonperiodic microstructures of plant tissues. The results obtained via this method satisfactorily obey the geometric, statistical, and topological laws of naturally evolved cellular solids. The predicted models are also validated by experimental data.

DOI: [10.1103/PhysRevE.86.031921](https://doi.org/10.1103/PhysRevE.86.031921)

PACS number(s): 87.85.Lf, 87.18.Fx, 87.64.-t, 07.05.Tp

I. INTRODUCTION

Plants and their organs frequently exhibit excellent mechanical features that can inspire the development of novel technology and products. The study of their constituent materials, structural attributes, and physical properties is thus increasingly interesting to scientists and engineers. A plant organ is generally composed of an assembly of cellular tissues which make up its microstructure and largely govern its physical properties. Each tissue has evolved to meet specific functional requirements that guarantee plant survival in a given environment. The way in which multiple tissues are geometrically tessellated within an organ helps determine mechanical performance and is important for achieving optimal structural support. It has been demonstrated that the shape, size, and spatial distribution of cells governs the physical, biological, and structural properties of a cellular material [1,2]. Hence, the ability to realistically model the cellular microstructure of a plant tissue is crucial to the understanding of its mechanical behavior [3].

Cellular structures in plants may appear quasiregular and periodic. For example, cork and balsa wood are almost as regular as honeycomb [4]. This type of structure can be modeled using a repeated unit cell with a given geometric shape. While important for analyzing the microstructure of periodic cellular solids, this method cannot account for the structural variations and imperfections inherent to most natural cellular solids. An alternative technique, the Voronoi

tessellation, can be used to generate an accurate representation of a nonperiodic microstructure [5–7]. In previous works, however, the actual cellular distribution of a natural structure has not been considered in the generation of the virtual model. In fact, the nucleation points of the Voronoi cells were generated randomly, thereby yielding a structure that differed significantly from the actual cell distribution of a real plant tissue. Nevertheless, the structural analyses of these Voronoi models delineated the dependence of the mechanical properties on the randomness of nonperiodic microstructures.

A Voronoi tessellation is a partition or tiling of a d -dimensional space into d -dimensional polyhedral cells. Such technique has been applied in numerous fields including biology, meteorology, metallurgy, crystallography, forestry, ecology, geology, geography, computer science, and engineering [8–10]. Because of its capacity to capture the randomness of a cellular pattern, this technique can be applied to model a plant tissue, with its irregular cell shapes and sizes. A Voronoi tessellation requires a partition of a given d -dimensional space such that the distances between the points of a cell and its center are minimized. Voronoi tessellation is extensively used to model grain geometry for the characterization of the properties of polycrystalline aggregates [11] and intergranular cracks [12]. Mattea *et al.* [13] and Roudot *et al.* [14] pioneered the use of Voronoi tessellation to model the microstructure of fruit tissues. However, neither group was able to generate a representative geometrical model that resembled the actual tissue micrograph. Both groups aimed only to capture the randomness of the fruit tissue microstructure without necessarily producing a model that accurately represents the real tissue. Mebatsion *et al.* [15] applied a Voronoi algorithm to model the parenchyma tissue of different apple cultivars. They developed virtual models using centroid-based Voronoi tessellation (CVT) and Poisson Voronoi tessellation (PVT), the latter model bearing a closer resemblance to the actual

*tanvir.faisal@mail.mcgill.ca

†nicolay.hristozov@mail.mcgill.ca

‡alejandro.rey@mcgill.ca

§tamara.western@mcgill.ca

||Corresponding author: damiano.pasini@mcgill.ca

fruit parenchyma. Also in this work, however, the technique is unable to differentiate between the actual cells and the extracellular spaces that are present in the tissue. Moreover, the cells are more elliptical in fruit parenchyma compared to those in plant petiole and stem. Mebatsion *et al.* later developed a new modeling technique, the ellipse tessellation, which was able to generate a more accurate representation of the fruit parenchyma [15,16].

This work is a part of a larger project which aims at not only modeling the microstructure of plant tissues but also characterizing their mechanical properties [17], the subject of future work. The need to develop a realistic geometric model of the plant tissues is crucial to understanding tissue mechanics since certain mechanical properties are governed by the architecture and structural distribution of the tissue. Given that stem and petiole tissues are morphologically different from fruit parenchyma, the Voronoi tessellation, specifically the CVT, can be an appropriate modeling tool. However, in a recent publication, Ntenga and Beakou [18,19] tried to analyze the structure, morphology, and mechanical properties of *Rhizophyllum camerunense* (RC) plant fiber using a conventional Voronoi diagram. Due to inherent drawbacks in the Voronoi (CVT) model, semi-infinite edges were present at the boundary of the fiber, making the model unsuitable for finite element analysis (FEA). To overcome this challenge, Ntenga and Beakou developed a virtual model coupled with a java-based image-processing program, IMAGEJ. This method can be used to model an arrangement of cells bounded by an irregular shape; however, one requirement for its application is that the edges at the sample boundary need to be reconstructed to obtain straight line edges.

The conventional CVT has the drawback that it yields semi-infinite edges at the boundary. As a result, the mechanical response of a microstructure with an irregular shape contour is impossible to calculate. The main objective of this work is the development of a comprehensive CVT-based technique for generating geometric models that possess finite edges at the sample boundary. The method is applied to model the tissue microstructure using the image data of two species, the dicot *Arabidopsis thaliana* and the monocot *Philodendron melinonii*, which have inherently different tissue architecture with regards to the placement of vascular tissue, as well as the production of atypical aerenchyma by *P. melinonii*. The method introduced here allows the modeling of a microstructure defined by a boundary of any irregular or regular shape. It is here applied to model microstructures defined by a boundary of either wedge-shape, or circular, or rectangular form, displaying a highly nonperiodic cellular gradient. The results are partially validated by topological laws as well as experimental data.

II. MATERIALS AND METHODS

Although this work focuses primarily on the geometrical modeling of plant tissues, the ultimate goal is to capture the contribution of tissue microstructure to the structural behavior of petioles and stems. Hence, while the technique presented here is a generalized way to model plant microstructure, the models have been generated with the aim of capturing the mechanics of these organs through FEA.

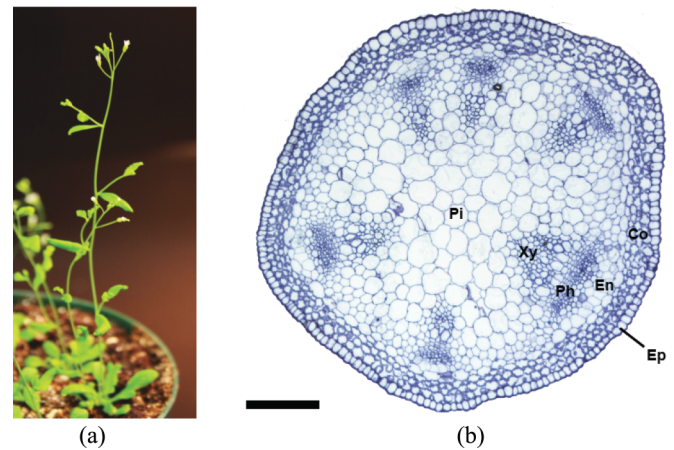


FIG. 1. (Color online) (a) Maturing *Arabidopsis thaliana* plant. (b) Micrograph of transversely sectioned *Arabidopsis* stem stained with toluidine blue. Pith (Pi), xylem (Xy), phloem (Ph), endodermis (En), cortex (Co), and epidermis (Ep) tissues are visible. Scale bar = 300 μm .

A. Model plant species

Arabidopsis thaliana, shown in Fig. 1, is a flowering plant that has become very popular as a model organism in genetics and molecular biology [20]. It is a terrestrial plant, whose primary inflorescence stem grows to a height of about 30 cm. The small size, brief life cycle, and high fertility of *Arabidopsis* make it amenable to rapid and large-scale experimentation. Furthermore, the availability of thousands of mutant lines makes it relatively trivial to grow plants that display subtle architectural differences.

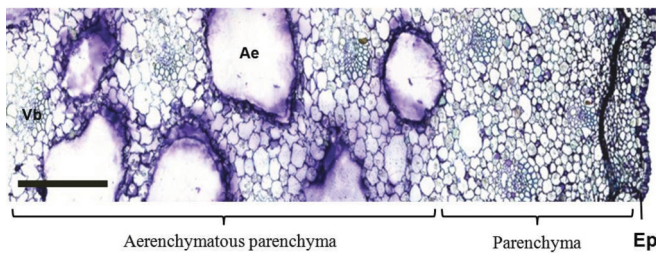
Philodendron melinonii is a relatively rare tropical plant that is substantially larger in size, with petioles measuring up to 1 m in length (Fig. 2). These petioles must support large, heavy leaves against physical stresses such as wind and precipitation. Aside from being lightweight and very stiff, *P. melinonii* petioles display two unusual structural adaptations: an aerenchymatous core and a broad, flat groove along the apical surface. Aerenchymatous tissues are normally found in the roots of aquatic plants, where they aid in gas exchange. In their study of two related species, Hejnowicz and Barthlott [21] reason that aerenchymae such as these primarily serve a structural role, reducing the density and energetic cost of these large petioles. The apical groove, meanwhile, gives the petiole a peculiar D-shaped cross-section which may contribute to its mechanical anisotropy. We examine these two species, whose cellular structures are very dissimilar, to demonstrate the broad applicability of FECVT in tissue modeling.

B. Growth conditions, sample preparation, and image acquisition

Arabidopsis thaliana seeds were planted on solid AT media [22] and stratified at 4 °C for 2–5 days. They were grown at 22 °C under continuous light before being transplanted onto soil after 7–10 days. Stem segments were harvested at ~5 weeks. Short segments from below the shoot apical meristem were fixed in 0.5% glutaraldehyde, dehydrated, and embedded in Spurr's resin as described in Western *et al.* [23]. These were cut into 1000-nm sections which were then stained with 1%



(a)



(b)

FIG. 2. (Color online) (a) Adult *Philodendron melinonii* plant. (b) Micrograph of transversely sectioned *P. melinonii* petiole stained with toluidine blue. Aerenchyma (Ae) and vascular bundles (Vb) are visible, as are three tissue layers: epidermis (Ep), parenchyma, and aerenchymatous parenchyma. Scale bar = 1 mm.

toluidine blue O in 1% sodium borate. Images were acquired with a Leica DM6000B microscope using OPENLAB [Fig. 1(b)]. In order to obtain high-resolution images of stems, individual stem sections had to be photographed in pieces (e.g., one photograph for the top half of the stem section and a second to capture the bottom half of the section). These photographs were digitally stitched together to form composite images using Adobe Photoshop.

Fresh *Philodendron melinonii* petioles were collected from the Montreal Botanical Garden. Small slices of petiole were fixed in formaldehyde : acetic acid : alcohol (FAA), dehydrated, and embedded in Paraplast Plus as described by Ruzin [24]. These were cut into 8- μ m sections and stained with 0.05% toluidine blue O in sodium citrate. Sections were imaged as above [Fig. 2(b)].

C. Voronoi tessellation technique

Given two points p_1 and p_2 , their Voronoi regions in the plane are the two regions on either side of the perpendicular bisector of the line segment joining p_1 and p_2 [Fig. 3(a)]. This bisector is the boundary edge of the Voronoi region. A Voronoi microstructure is constructed based on a set of randomly generated points called Voronoi sites. The cell boundaries are drawn such that any point within the enclosed polygon is closer to its Voronoi site than to the Voronoi sites of the surrounding polygons. The Voronoi tessellation thus divides a space into

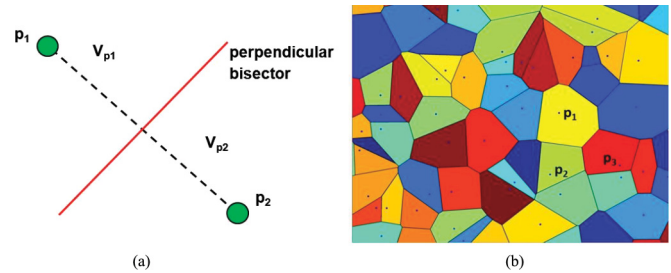


FIG. 3. (Color online) (a) Schematic illustrating the creation of two Voronoi domains through the perpendicular bisector (solid line) of the line segments joining p_1 and p_2 . (b) 2D Voronoi region generated for 50 randomly generated Voronoi sites.

as many regions as there are Voronoi sites [Fig. 3(b)]. Usually in a two-dimensional space, two methods are used to generate a Voronoi diagram. One is known as PVT, where points are randomly distributed in space according to the Poisson point process. The second one is the CVT, where the centroids of the cells are used to construct the Voronoi diagram.

In a CVT, the associated generating points are centroids (center of mass with respect to a given density function) of the corresponding Voronoi cells. For a given domain $D \subseteq \mathbb{R}^N$ and a density function $\rho(x)$ defined for $x \in D$, the center of mass or centroid z_c of D is given by

$$z_c = \frac{\int_D x \rho(x) dx}{\int_D \rho(x) dx}. \quad (1)$$

If an object has uniform density, its center of mass is the same as the centroid of its shape. When the centroids of the cells and Voronoi sites coincide, the resulting diagram is called CVT.

D. Generation of a conventional CVT

1. Image segmentation

To model the microstructure, we need to calculate the centroids of the cells present in a micrograph. This begins with the segmentation of a color micrograph of plant tissue. Segmentation refers to the process of partitioning a digital image into multiple segments [25]. The goal of this process is to simplify both the representation of an image and its analysis. It helps to distinguish the cells and the cell boundaries from the background. The simplest method for image segmentation is known as “thresholding.” Based on an optimum threshold value, thresholding converts a color or gray-scale image into a binary (black and white) image. Thresholding is performed here using Otsu’s method [26], a well-known algorithm for global thresholding. The interclass variance of black and white pixels of the binary image is minimized to compute a global threshold value, which is a normalized value between 0 and 1.

2. Edge detection

Since plant tissue microstructures exhibit graded cellularity as well as complex heterogeneity, thresholding is not sufficient to identify the cells in a micrograph. An edge detection algorithm is used in conjunction with thresholding to obtain the cellular distribution accurately. The Canny edge detection algorithm, which uses double thresholding, is applied here

because it can detect true but weak edges [27]. In this algorithm, the noise is first removed to smooth the image. Next, the edge detector finds the image gradient to highlight regions with spatial derivatives. The regions are tracked and the pixel that is not at the maximum is suppressed. The gradient array is then reduced by hysteresis, which is used to trace the remaining pixels that have not been suppressed. The hysteresis uses two thresholds and is set to zero (nonedge) if the magnitude is below the first threshold. The edge is created if the magnitude is above the high threshold. However, if the magnitude is between the two thresholds, it is set to zero unless there is a path from this pixel to a pixel with a gradient above the higher threshold. As a result, the shape of the cell can be detected more precisely.

3. Calculation of centroids

The calculation of centroids depends on the *region of interest* [28], a region of nonzero pixel value, which is 1 for a binary image. Based on x and y coordinates of the pixels, the first-order moments of the cells are computed. Since we are working with a digital image, the moment equation is modified into the following algebraic form:

$$m_{pq} = \sum_{i=1}^{n_1} \sum_{j=1}^{n_2} x_i^p y_j^q f(i, j), \tag{2}$$

where (x_i, y_j) is the coordinate of the i, j th pixel, $f(i, j)$ have value 1 if the i, j th pixel is in the shape and 0 otherwise. Considering the region of interest, which is completely enclosed in a rectangular region G of size n_1 by n_2 pixels, i varies from 1 to n_1 and j varies from 1 to n_2 in the function $f(i, j)$. For a two-dimensional (2D) region, $p + q$ denotes the order of moment, where p and q are integers.

The coordinates of a cell are

$$\bar{x} = \frac{m_{10}}{m_{00}} \quad \text{and} \quad \bar{y} = \frac{m_{01}}{m_{00}}, \tag{3}$$

where the zeroth moment, physically, is equal to the area of the region.

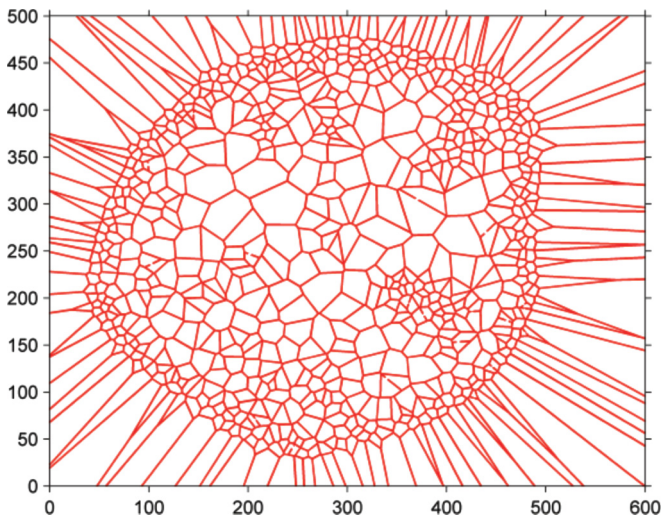


FIG. 4. (Color online) *Arabidopsis* stem modeled with the conventional Voronoi tessellation. The unrealistic semi-infinite edges appearing at the boundary of the figures are a limitation of this method.

4. Generation of CVT

After determining the centroids of the cells, which are the Voronoi sites, the Voronoi tessellation is constructed based on the QuickHull algorithm [29]. The outcome is a CVT (Fig. 4) with semi-infinite edges at the boundary. Furthermore, while there may be a clear boundary in the micrograph, there is no specific boundary in the corresponding Voronoi model. The semi-infinite edges complicate finite element analysis because the boundary conditions, applied at an infinite distance, are not realistic. This problem is especially difficult to correct in models with irregular shape contour.

E. Finite-edge centroidal Voronoi tessellation (FECVT)

Conventional CVT is not sufficient to represent a microstructure with an arbitrary shape contour. To remove the infinite edges from the boundary, the centroids of the outermost cells should be determined. For each centroid, the distances between the centroid and the surrounding Voronoi sites (centroids of the surrounding polygons) are calculated and the minimum distance is determined. An imaginary point is created such that the distance between itself and the centroid is half of the minimum distance. The imaginary point is thus created for each of the selected centroids. The purpose of generating the imaginary points is to create a boundary using convex hull algorithm [29]. If a finite planar set of points is given, the convex set of minimum area, which contains the original set, is known as the convex hull. In computational geometry, especially in computer graphics and image processing, the set usually consists of n points (in two or higher dimensions). In two dimensions, a convex hull is the minimal polygon that encloses all the given points. Based on the set of imaginary points and the convex hull algorithm, a boundary is imposed, after which a Boolean subtraction is realized. With this Boolean operation, the semi-infinite edges are truncated and the vertices of the truncated edges are reconnected to form the final boundary. Hence, the semi-infinite edges are removed, and straight line edges are obtained to create cell boundaries. The finite-edge centroidal Voronoi tessellation (FECVT) technique is thus capable of capturing the microstructure of an image with an arbitrarily shaped boundary contour.

III. RESULTS AND DISCUSSION

Arabidopsis, a dicotyledon, displays a complex stem structure consisting of several tissue layers [Fig. 1(b)]. The core

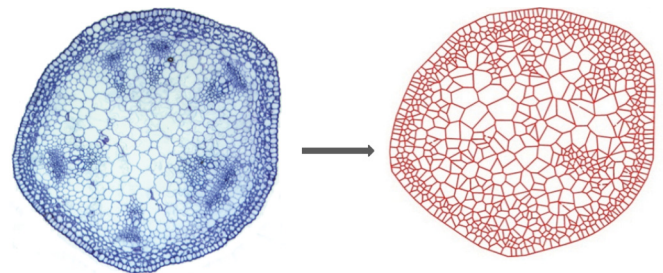


FIG. 5. (Color online) FECVT model of the entire cross section of *Arabidopsis* stem.

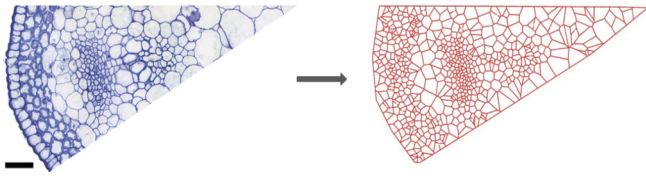


FIG. 6. (Color online) FECVT model of a wedge section of the *Arabidopsis* stem. Scale bar = 100 μm .

of the stem is composed of pith, a foamlike tissue composed of large, thin-walled parenchyma cells. Surrounding this core is a ring of fibrous xylem and interfascicular fibers, which functions as the stem's main structural support. Outside this layer lie the phloem, the endodermis, and a thick layer of cortical cells. An epidermal monolayer then surrounds the entire stem. Although six types of tissues were identified, the cross section of the inflorescence stem of *Arabidopsis thaliana* displays mainly three layers of tissues. The outer layer consists of epidermis (Ep), cortex (Co), primary phloem (Ph), the middle layer is comprised of primary xylem (Xy) and interfascicular fiber tissue (if any), and the inner layer represents pith (Pi). These layers of tissues are used to define the stem's mechanical architecture and response to mechanical perturbation [30]. The goal of the present work is to capture the cellular distribution within a plant petiole or stem; the results will be used in a future work to find out the structural effects of the cellular microstructures, determining the overall mechanical properties. The overall aim is to understand how the natural cellular microstructure affects the overall mechanical properties of a hierarchic cellular structure. Since the method captures the cellular variations in its virtual model, it is representative of the original cellular structure. This relatively complex microstructure was modeled using the FECVT method (Fig. 5). The FECVT model represents the stem realistically, in a sense, capturing the geometry of the cellular tissues. Using higher magnification to capture more structural detail, a wedge-shaped portion of the *Arabidopsis* stem was also modeled using the FECVT method (Fig. 6).

P. melinonii, a monocotyledon, displays relatively simple structural organization [Fig. 2(b)]. The interior of the petiole

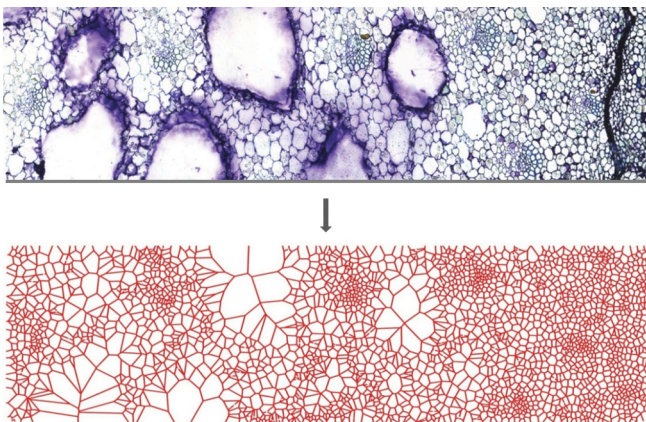
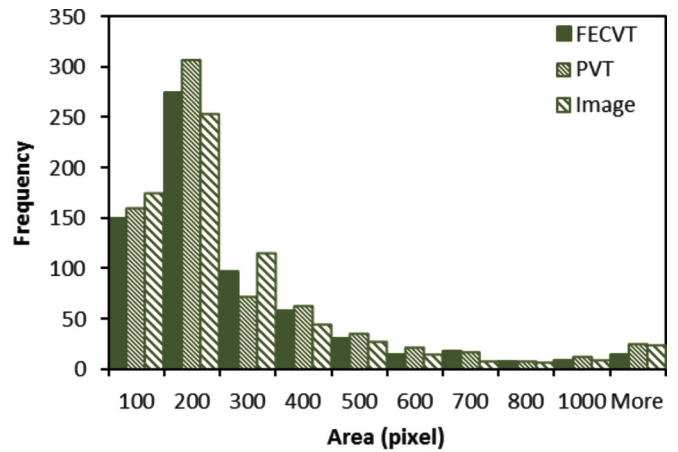
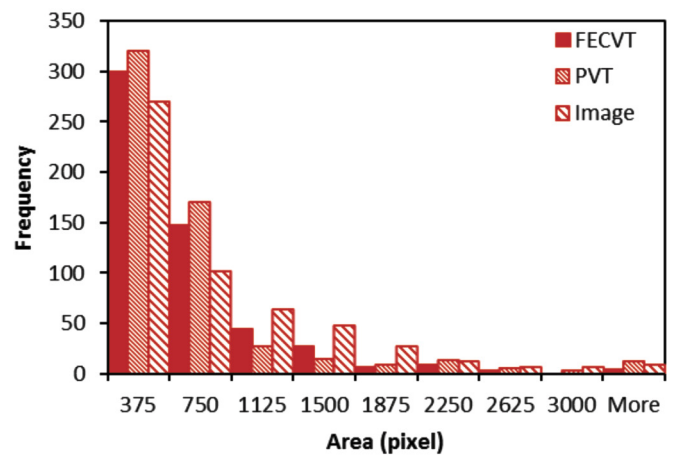


FIG. 7. (Color online) FECVT model of an extract of the cross section from a *P. melinonii* petiole.

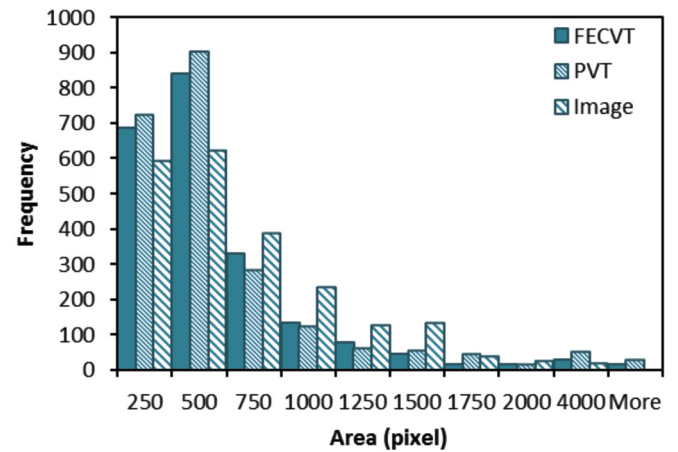
is composed almost entirely of parenchyma cells. There is a steady gradation in cell size, with the outermost cells being the smallest and the innermost cells being the largest.



(a) Entire *Arabidopsis* stem



(b) Wedge section of *Arabidopsis* stem



(c) A section of *P. melinonii* petiole

FIG. 8. (Color online) Cellular area distribution of tissue images and corresponding FECVT and PVT models of entire *Arabidopsis* stem (a), partial *Arabidopsis* stem, (b) and a section of *P. melinonii* petiole (c).

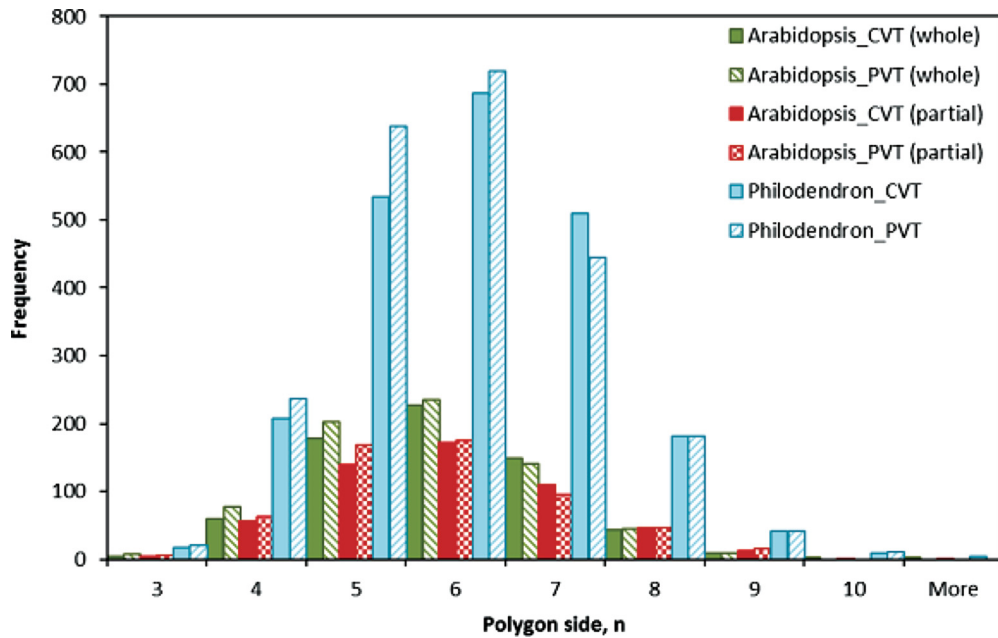


FIG. 9. (Color online) Frequency distributions of the polygon side of the FECVT and PVT models for the entire *Arabidopsis* [the solid green (gray) and the downward diagonal], partial *Arabidopsis* [the solid red (dark gray) and the checker board] stem, and a portion of the cross section of the *P. melinonii* [the solid aqua (light gray) and the upward diagonal] petiole. The average number of sides in the FECVT models varies from 5.91 to 5.96; for the PVT models, on the other hand, it ranges between 5.86 and 5.92.

Vascular bundles, which contain stiff xylem cells, are scattered randomly throughout this parenchymatous tissue. Once again, an epidermal monolayer surrounds the entire structure. The FECVT model of the *P. melinonii* petiole is shown in Fig. 7. Since experimental data are used to formulate the mathematical model, the accuracy of the model appears to depend on the quality of the micrograph. Both the *Arabidopsis* and *P. melinonii* tissue micrographs are used to generate the respective FECVT models. The FECVT method, thus, can capture the detail of cellular distribution if the micrograph of the tissue microstructure is vivid and clear. However, the polygons at the boundary of an FECVT model may differ in shape and size from the boundary polygons of a conventional CVT. We note here that the aerenchyma cells in the FECVT model partially match the real tissue, since each of the aerenchyma cells is represented by more than one cell. As a result of the staining process, the cells were stained with toluidine blue O, and thus the aerenchyma cells were also colored. Hence, during the image processing, each aerenchyma appeared to be broken up into multiple cells. The boundaries of these cells can be easily removed manually to form larger aerenchyma cells. This will be done in a future work, when a finite element analysis of the tissue is carried out.

The application of the Canny edge detection algorithm significantly enhances the accuracy of detecting the cell boundaries. In the previous works [15,19], the tissue microstructures were less complex in terms of variation of cell shape and size and did not display an intense cellular gradient. On the other hand, the microstructures examined in this work are highly nonperiodic and heterogeneous [Figs. 1(b) and 2(b)], displaying remarkable cellular gradients. In the virtual geometric models, the FECVT method shows its ability to capture this complex heterogeneity and the graded cellularity.

The statistical characteristics are shown in Figs. 8–13. In Fig. 8, both the original micrographs and the virtual models (i.e., FECVT and PVT models) are considered, whereas in the other figures, the characteristics are shown only for the virtual models. The cell areas of the *Arabidopsis* and *P. melinonii* tissues are determined using the image micrographs, and the area distributions are used to validate the FECVT models. In the original micrographs, the cell areas are calculated using digital image processing based on the pixel information. The

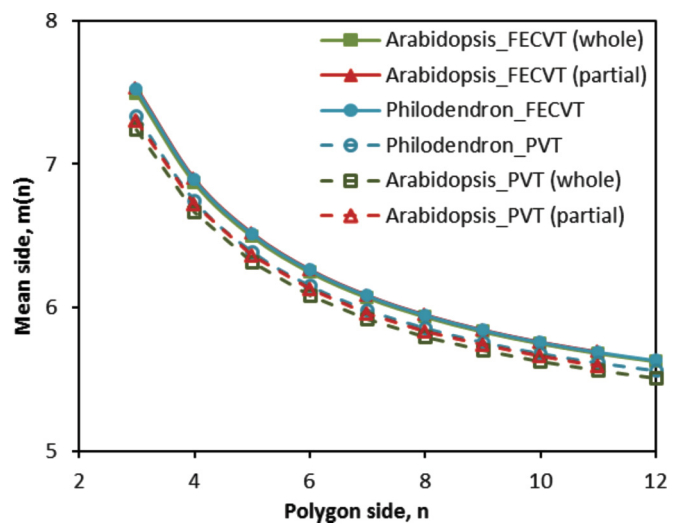


FIG. 10. (Color online) Polygons of fewer sides are surrounded by the polygons of more sides for different FECVT and PVT models. In naturally evolved cellular structures, the few-edged cell has a tendency to be in contact with several-edged cells and vice versa [33,34].

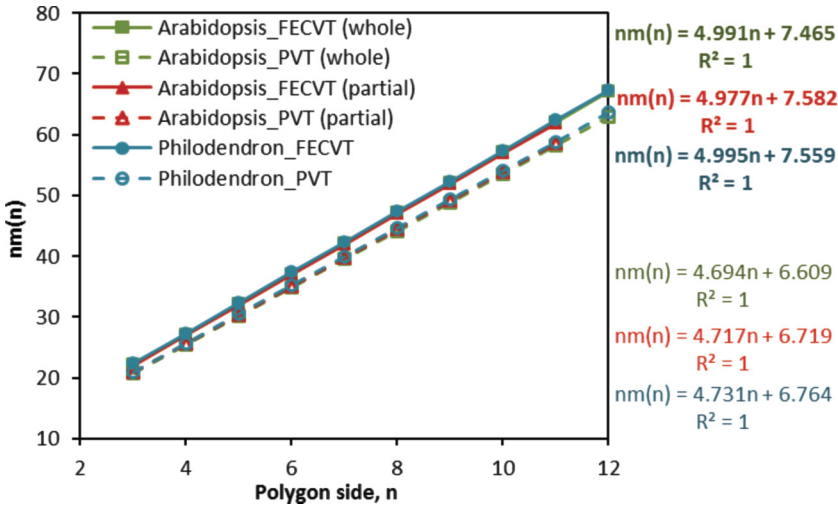


FIG. 11. (Color online) Aboav-Weaire law for 2D topology. A linear relation between the mean cell sides to the neighboring cell sides for a random cellular structure. The upper three equations in bold represent FECVT models and the lower three equations represent PVT models.

cell areas from the different images and their corresponding FECVT and PVT models are statistically compared in Fig. 8. It is reflected in this figure that the variations of cell area distributions of the FECVT and PVT models are subtle. The cell area distributions for both the models conform to the distributions of the corresponding image area. By contrast, in a conventional Voronoi model with semi-infinite edges, the areas of the virtual cells differ significantly with respect to the original images since the boundary cell areas are large due to semi-infinite edges. Figure 9 depicts the frequency distribution of polygon shapes in different FECVT and PVT models. Although both the FECVT and PVT methods create cells with more than ten edges, we do not see such cell shapes in the original micrographs. However, in contrast to PVT models, the FECVT models are inclined to be hexagon dominated where five-sided polygons are counterbalanced by seven-sided polygons. The FECVT models display geometric randomness, but they strongly tend to follow Euler’s law, which relates the number of vertices V , edges E , and faces F of cells. As a consequence of Euler’s law, an irregular honeycomb with an edge connectivity of 3 should have, on average, six sides per face. For a honeycomb with regular hexagonal cells, the average number of sides is $\langle n \rangle = 6$; in these centroidal Voronoi models, $\langle n \rangle$ varies from 5.91 to 5.96 while for the PVT models, $\langle n \rangle$ varies from 5.86 to 5.92. Comparing the average cell sides between the two types of models, the FECVT models have the tendency to follow Euler’s law more strongly.

Biological tissues, soap bubbles, and polycrystalline grains are natural examples of random, space-filling cellular networks. Despite large differences in length scales and formation processes, all these cellular networks evolve to a steady state with a similar structure. In most systems, the pinning of boundaries by surface grooving leads to stagnation of grain or tissue growth. This can be characterized by measuring the spatial distribution of cell sizes, shapes, and their geometric correlations. There is a strong correlation between the microstructural geometry and the structural properties of space-filling networks. The interdependence between topology, geometry, and physical dynamics of the spherulitic grain size-shape arrangement in semi-crystalline polymeric cellular networks has been shown both experimentally and

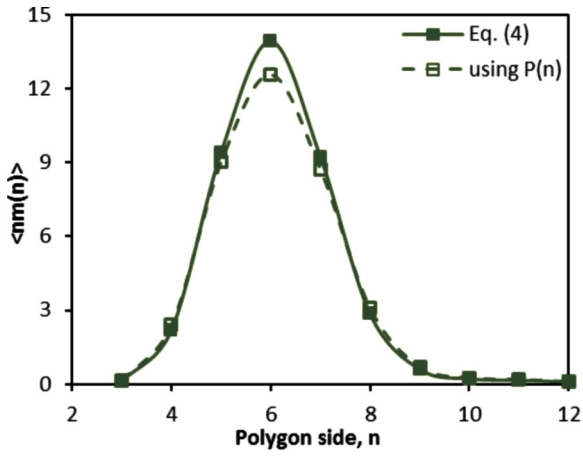
theoretically [31,32]. In naturally evolved cellular structures, the few-edged cell has a tendency to be in contact with many-edged cells and vice versa [33,34]. Since the FECVT models represent plant tissues, they are expected to follow this spatial distribution. In Fig. 10, we observe that polygons with fewer sides tend to be surrounded by polygons with more sides and that this holds true for all the models generated by both the FECVT and PVT methods. We expect similar trends for both types of models, since only the distribution of the points is different in the Poisson Voronoi tessellation. Aboav-Weaire [33,35] established a linear relationship between the mean cell sides and the neighboring cell sides for an infinite random cellular structure. This correlation is empirical and is satisfied by a large number of naturally grown cellular structures. According to the Aboav-Weaire law, on average, the sum of the number of sides of the cells immediately adjacent to an n -sided cell, $nm(n)$ is linear in n such that

$$nm(n) = (6 - a)n + (6a + \mu_2), \quad (4)$$

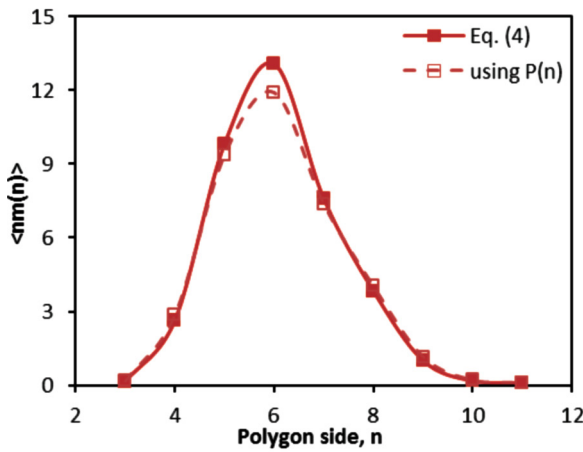
where μ_2 is the second moment of the $P(n)$, the probability distribution of the number of edges and a , a system constant, is a measure of nearest neighbor correlation that depends on the topology. Generally, in biological structures, a is in the order of 1 [36,37]. The second moment is defined as $\mu_2 = \sum_n P(n)(n - \langle n \rangle)^2$, where $\langle n \rangle$ is the average with respect to the same distribution, $P(n)$, and whose variance, $\text{var}(n) = (\langle n^2 \rangle - \langle n \rangle^2)$ is a measure of topological disorder. However, for finite networks with $\langle n \rangle \neq 6$, the topological model yields the relation

$$nm(n) = (\langle n \rangle - a)n + [\langle nm(n) \rangle - \langle n \rangle^2 + \langle n \rangle a]. \quad (5)$$

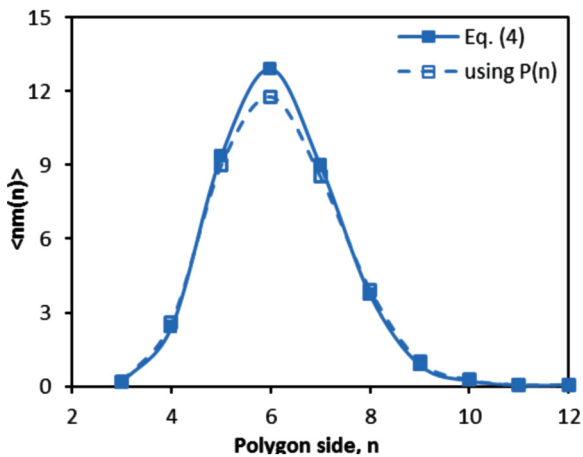
A wide range of experiments conducted on various natural structures have demonstrated that their cellular geometries obey the above correlations [33,36–38]. In Fig. 11, the tessellated models for both the FECVT and PVT methods display a linear relationship between the mean sides of the polygonal cells and the surrounding cells. For the FECVT models, $a \approx 1$, whereas for the PVT models, $a \approx 1.3$. The parameter a quantifies the deviation of the slope from the average number of sides. Hence, the FECVT method is apparently an appropriate tool for generating virtual models



(a) Entire *Arabidopsis* stem



(b) Wedge section of *Arabidopsis* stem



(c) A section of *P. melinonii* petiole

FIG. 12. (Color online) Comparison of the parameter $\langle nm(n) \rangle$, for the FECVT models, obtained through the modified Aboav-Weaire law [Eq. (4)] for 2D finite networks, and the probability distribution of the polygonal cells for the respective models. The consistency of the parameter $\langle nm(n) \rangle$ is shown.

of plant tissues. Furthermore, the consistency of the Aboav-Weaire law for finite networks [Eq. (5)] is verified, calculating $\langle nm(n) \rangle$ using $P(n)$ of the FECVT models shown in Fig. 9.

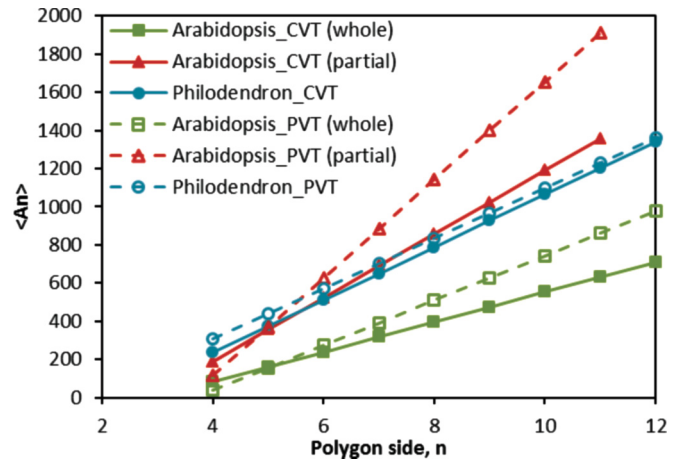


FIG. 13. (Color online) Relations between the average area of cells and the number of polygon sides for the FECVT and PVT models. The linear relationship between cell size (area), stated in Lewis’s law, holds true for biological tissues and various cellular networks.

Using the results for a , $\langle n \rangle$, and the intercept shown in Fig. 11, $\langle nm(n) \rangle$ is calculated from Eq. (5). The results are consistent for both the *Arabidopsis* and *P. melinonii* tissues and are shown in Fig. 12.

Another useful statistical measure, Lewis’s law, states that the average area of a polygon with n sides $\langle A_n \rangle$ should be a linear function of the number of sides n , which holds true for various cellular networks and biological tissues [33,34,39–41]:

$$\langle A_n \rangle = \langle A \rangle [1 + \lambda(n - 6)], \quad n \geq 3 \quad (6)$$

where λ is a constant and usually, $\lambda = 1/4$ for a Voronoi tessellation [42]. Mombach *et al.* [43] investigated five different epidermal vegetable tissues and found the values of λ in the range of 0.16–0.23. Figure 13 shows the correlation between the sizes and shapes of the cells for the FECVT models and the corresponding PVT models. In the virtual tissues (Voronoi models) generated by both of the methods, as expected, the average area $\langle A_n \rangle$ of the n -sided cells varies monotonically with varying n . In the FECVT models, λ varies from 0.27 to 0.33, whereas in the PVT models, λ varies from 0.23 to 0.43. Speculatively, we can say λ is influenced by the dispersion of cell areas as well as the number of cells. The values of λ for the FECVT models are close to its usual value [42].

Topologically, the shape of the Voronoi polygons is considered to be a random variable. The polygons cannot be defined and distinguished by their sizes or any other metric measures alone. For this reason, we can use topological entropy as a measure of randomness, i.e., a statistical measure of a disordered pattern. The topological entropy S_t is defined as $S_t = -\sum_n p_n \ln(p_n)$, where $S_t \geq 0$ and p_n is the probability of finding n -sided polygons within a Voronoi diagram. For perfectly regular and periodic patterns, the topological entropy is zero. It increases with the increasing randomness of the polygons in a region of interest [8]. The image entropies of the whole and partial *Arabidopsis* micrographs are 2.1624 and 1.8456, respectively, while the corresponding FECVT models’ entropies are 1.8187 and 1.6658, respectively. In contrast with

FECVT, the PVT models' entropies are 1.5995 and 1.6421, respectively. The image entropy is calculated from a gray-scale image derived from a color micrograph. The entropic variation between the image and its model is partly due to the conversion of the image to gray scale and also to the original quality of the micrograph. For the high-magnification wedge-shaped micrograph, the image entropy and FECVT model entropy are closer to each other. Cell boundaries tend to appear sharper under higher magnification, which allows the corresponding FECVT model to be as random as the natural microstructure. In case of the *P. melinonii* petiole, the image entropy and the FECVT, and PVT models entropies are 1.7141, 1.6223, and 1.6191, respectively. The difference between the image entropy and model entropy is narrower for *P. melinonii* due to the larger number of cells and the higher image quality. However, for both species, FECVT model entropies are close to the corresponding image entropies comparing with PVT models. These statistical analyses demonstrate the applicability of the FECVT method to a range of different tissue microstructures. We emphasize, however, that the accuracy of the model in capturing the microstructure is highly dependent on the quality, resolution, and magnification of the micrograph.

IV. CONCLUSION AND FUTURE WORKS

The goal of this work is to generate a Voronoi model that can realistically capture the microstructure of plant tissues. To demonstrate the effective application of the FECVT method, two distinct and complex nonperiodic structures displaying graded cellularity have been modeled. The predicted FECVT models are partially validated by topological laws as well as experimental data and compared with PVT models. A number of statistical and topological analyses manifest the appropriateness of the FECVT method in modeling plant tissues.

Furthermore, the purpose of this work is not only constructing Voronoi diagrams but to give a realistic representation of plant cellular tissues. The FECVT method can be used to capture the microstructure of any shape in which the tissues display complex heterogeneity and graded cellularity. The use of an edge detection algorithm augments the ability of the FECVT method to capture these types of geometries. The model can be generated using MATLAB without the assistance of any other image processing software and can be integrated directly with FEA software (ANSYS) without the need for preprocessing. Additionally, the FECVT method can generate a model with finite edges, making it easier to study the mechanics of the structure using FEA. The geometric models are representative of the structures they mimic and allow us to computationally model the elastic properties of a cellular tissue with higher accuracy. The geometrical representation of a tissue can help enhance our understanding of how microstructure determines mechanical properties. It can also help us to develop predictive models of known mechanical behavior.

ACKNOWLEDGMENTS

The authors would like to thank the staff and administration of the Montreal Botanical Garden for donating the *P. melinonii* petioles, in particular Marc-Stéphane Bailleul, Renée Gaudette, Hélène Giguere, and Lise Lacouture. The authors also thank Dr. Denis Barabé and Dr. Anja Geitmann for their assistance in acquiring these samples. Finally, the authors thank Heather McFarlane, Bronwen Forward, and Dr. Thomas Bureau for their help with microscopy. This research is supported by a grant from Fonds de recherche du Québec—Nature et technologies (FQRNT). The authors thank the reviewers for their valuable comments and suggestions.

-
- [1] S. Ghosh, K. Lee, and S. Moorthy, *Comput. Methods Appl. Mech. Eng.* **132**, 63 (1996).
 - [2] D. Pasini, *Journal of Design & Nature and Ecodynamics* **3**, 1 (2008).
 - [3] T. R. Faisal, E. M. Khalil Abad, N. Hristozov, and D. Pasini, *J. Bionic Eng.* **7**, 11S (2010).
 - [4] L. J. Gibson and M. F. Ashby, *Cellular Solids: Structure and Properties*, 2nd ed., Cambridge Solid State Science series (Cambridge University Press, Cambridge, New York, 1999).
 - [5] K. Li, X. L. Gao, and G. Subhash, *Int. J. Solids Struct.* **42**, 1777 (2005).
 - [6] M. J. Silva and L. J. Gibson, *Int. J. Mech. Sci.* **39**, 549 (1997).
 - [7] M. J. Silva, W. C. Hayes, and L. J. Gibson, *Int. J. Mech. Sci.* **37**, 1161 (1995).
 - [8] A. Okabe, B. Boots, K. Sugihara, and S. N. Chiu, *Spatial Tessellations: Concepts and Applications of Voronoi Diagrams*, 2nd ed. (John Wiley & Sons, New York, 2000).
 - [9] J. A. Blackman and P. A. Mulheran, *Phys. Rev. B* **54**, 11681 (1996).
 - [10] D. L. González, A. Pimpinelli, and T. L. Einstein, *Phys. Rev. E* **84**, 011601 (2011).
 - [11] G. Cailletaud, S. Forest, D. Jeulin, F. Feyel, I. Galliet, V. Mounoury, and S. Quilici, *Comput. Mater. Sci.* **27**, 351 (2003).
 - [12] K. Hussain, E. R. De los Rios, and A. Navarro, *Eng. Fract. Mech.* **44**, 425 (1993).
 - [13] M. Mattea, M. J. Urbicain, and E. Rotstein, *Chem. Eng. Sci.* **44**, 2853 (1989).
 - [14] A. C. Roudot, F. Duprat, and E. Pietri, *Food Struct.* **9**, 215 (1990).
 - [15] H. K. Mebatsion, P. Verboven, Q. T. Ho, F. Mendoza, B. E. Verlinden, T. A. Nguyen, and B. M. Nicolai, *Comput. Modeling Eng. Sci.* **14**, 1 (2006).
 - [16] H. K. Mebatsion, P. Verboven, Q. T. Ho, B. E. Verlinden, and B. M. Nicolai, *Trends in Food Sci. Technol.* **19**, 59 (2008).
 - [17] A. D. Rey, D. Pasini, and Y. K. Murugesan, in *Biomimetics: Nature-Based Innovation*, edited by Y. Bar-Cohen (CRC Press, Boca Raton, FL, 2011), pp. 131–168.
 - [18] R. Ntenga and A. Beakou, *Comput. Mater. Sci.* **50**, 1442 (2011).
 - [19] A. Beakou and R. Ntenga, *Comput. Mater. Sci.* **50**, 1550 (2011).
 - [20] M. Koornneef and D. Meinke, *Plant J.* **61**, 909 (2010).
 - [21] Z. Hejnowicz and W. Barthlott, *Am. J. Bot.* **92**, 391 (2005).

- [22] G. W. Haughn and C. Somerville, *Mol. Gen. Genet.* **204**, 430 (1986).
- [23] T. L. Western, J. Burn, W. L. Tan, D. J. Skinner, L. Martin-McCaffrey, B. A. Moffatt, and G. W. Haughn, *Plant Physiol.* **127**, 998 (2001).
- [24] S. E. Ruzin, *Plant Microtechnique and Microscopy* (Oxford University Press, New York, 1999).
- [25] R. M. Haralick and L. G. Shapiro, *Computer and Robot Vision*, 1st ed., Vol. 1 (Addison-Wesley Longman, Boston, 1992).
- [26] N. Otsu, *IEEE Trans. Systems, Man and Cybernetics* **9**, 61 (1979).
- [27] J. Canny, *IEEE Trans. Pattern Analysis and Machine Intelligence PAMI-8*, 679 (1986).
- [28] K. F. Mulchrone and K. R. Choudhury, *J. Struct. Geol.* **26**, 143 (2004).
- [29] C. B. Barber, D. P. Dobkin, and H. Huhdanpaa, *ACM Trans. Mathematical Software* **22**, 469 (1996).
- [30] J. Fahlen and L. Salmen, *Biomacromolecules* **6**, 433 (2005).
- [31] T. Huang, T. Tsuji, M. R. Kamal, and A. D. Rey, *J. Mater. Sci.* **34**, 4551 (1999).
- [32] M. R. Kamal, T. Huang, and A. D. Rey, *J. Mater. Sci.* **32**, 4085 (1997).
- [33] S. N. Chiu, *Mater. Charact.* **34**, 149 (1995).
- [34] F. T. Lewis, *The Anatomical Record* **50**, 235 (1931).
- [35] D. A. Aboav, *Metallography* **13**, 43 (1980).
- [36] J. C. M. Mombach, R. M. C. de Almeida, and J. R. Iglesias, *Phys. Rev. E* **47**, 3712 (1993).
- [37] J. C. M. Mombach, R. M. C. de Almeida, and J. R. Iglesias, *Phys. Rev. E* **48**, 598 (1993).
- [38] P. Pina and M. A. Fortes, *J. Phys. D: Appl. Phys.* **29**, 2507 (1996).
- [39] G. L. Caër and R. Delannay, *J. Phys.* **13**, 1777 (1993).
- [40] T. Huang, M. R. Kamal, and A. D. Rey, *J. Mater. Sci. Lett.* **14**, 220 (1995).
- [41] P. Pina, J. Saraiva, L. Bandeira, and J. Antunes, *Planet. Space Sci.* **56**, 1919 (2008).
- [42] P. A. Mulheran, *Acta Metall. Mater.* **42**, 3589 (1994).
- [43] J. C. M. Mombach, M. A. Z. Vasconcellos, and R. M. C. d. Almeida, *J. Phys. D: Appl. Phys.* **23**, 600 (1990).